MYC-dependent oxidative metabolism regulates osteoclastogenesis via nuclear receptor ERRα

Seyeon Bae, … , Marjolein van der Meulen, Kyung-Hyun Park-Min

Research Article   Bone biology

Osteoporosis is a metabolic bone disorder associated with compromised bone strength and an increased risk of fracture. Inhibition of the differentiation of bone-resorbing osteoclasts is an effective strategy for the treatment of osteoporosis. Prior work by our laboratory and others has shown that MYC promotes osteoclastogenesis in vitro, but the underlying mechanisms are not well understood. In addition, the in vivo importance of osteoclast-expressed MYC in physiological and pathological bone loss is not known. Here, we have demonstrated that deletion of *Myc* in osteoclasts increases bone mass and protects mice from ovariectomy-induced (OVX-induced) osteoporosis. Transcriptomic analysis revealed that MYC drives metabolic reprogramming during osteoclast differentiation and functions as a metabolic switch to an oxidative state. We identified a role for MYC action in the transcriptional induction of estrogen receptor–related receptor α (ERRα), a nuclear receptor that cooperates with the transcription factor nuclear factor of activated T cells, c1 (NFATc1) to drive osteoclastogenesis. Accordingly, pharmacological inhibition of ERRα attenuated OVX-induced bone loss in mice. Our findings highlight a MYC/ERRα pathway that contributes to physiological and pathological bone loss by integrating the MYC/ERRα axis to drive metabolic reprogramming during osteoclast differentiation.

Find the latest version:

https://jci.me/89935/pdf

MYC-dependent oxidative metabolism regulates osteoclastogenesis via nuclear receptor ERRα

Seyeon Bae,[1] Min Joon Lee,[1] Se Hwan Mun,[1] Eugenia G. Giannopoulou,[1,2] Vladimir Yong-Gonzalez,[3] Justin R. Cross,[3] Koichi Murata,[1] Vincent Giguère,[4] Marjolein van der Meulen,[5,6] and Kyung-Hyun Park-Min[1,7]

[1]Arthritis and Tissue Degeneration Program, David Z. Rosensweig Genomics Research Center, Hospital for Special Surgery, New York, New York, USA. [2]Biological Sciences Department, New York City College of Technology, City University of New York, Brooklyn, New York, USA. [3]Donald B. and Catherine C. Marron Cancer Metabolism Center, Memorial Sloan Kettering Cancer Center, New York, New York, USA. [4]Goodman Cancer Research Centre, McGill University, Montréal, Canada; Departments of Biochemistry, Medicine and Oncology, McGill University, Montréal, Canada. [5]Sibley School of Mechanical and Aerospace Engineering, Cornell University, Ithaca, New York, USA. [6]Musculoskeletal Integrity Program, Hospital for Special Surgery, New York, New York, USA. [7]Department of Medicine, Weill Cornell Medical College, New York, New York, USA.

Osteoporosis is a metabolic bone disorder associated with compromised bone strength and an increased risk of fracture. Inhibition of the differentiation of bone-resorbing osteoclasts is an effective strategy for the treatment of osteoporosis. Prior work by our laboratory and others has shown that MYC promotes osteoclastogenesis in vitro, but the underlying mechanisms are not well understood. In addition, the in vivo importance of osteoclast-expressed MYC in physiological and pathological bone loss is not known. Here, we have demonstrated that deletion of *Myc* in osteoclasts increases bone mass and protects mice from ovariectomy-induced (OVX-induced) osteoporosis. Transcriptomic analysis revealed that MYC drives metabolic reprogramming during osteoclast differentiation and functions as a metabolic switch to an oxidative state. We identified a role for MYC action in the transcriptional induction of estrogen receptor–related receptor α (ERRα), a nuclear receptor that cooperates with the transcription factor nuclear factor of activated T cells, c1 (NFATc1) to drive osteoclastogenesis. Accordingly, pharmacological inhibition of ERRα attenuated OVX-induced bone loss in mice. Our findings highlight a MYC/ERRα pathway that contributes to physiological and pathological bone loss by integrating the MYC/ERRα axis to drive metabolic reprogramming during osteoclast differentiation.

Introduction

MYC (also known as c-MYC) is a broadly acting transcription factor that regulates the differentiation and proliferation program of cells by multiple mechanisms including a transcriptional amplification of target genes (1–3). MYC deficiency in mice is embryonically lethal (4), and aberrant overexpression of MYC is found in human cancers (5). MYC has been implicated in in vitro osteoclastogenesis (6, 7), and we recently identified MYC as an important transcriptional factor of the RANKL-induced transcriptional program by directly regulating nuclear factor of activated T cells, c1 (NFATc1) in osteoclasts (8). However, the molecular and cellular mechanism by which MYC regulates osteoclastogenesis and the functional role of myeloid cell-specific MYC during physiological and pathological bone remodeling in vivo are not completely elucidated.

Osteoclasts are multinuclear giant cells responsible for bone resorption and are derived from the myeloid lineage cells in response to RANKL (9, 10). RANKL activates canonical signaling pathways including NF-κB and MAPK as well as immunoreceptor tyrosine–

based activation motif (ITAM) immunoreceptor signaling pathways, synergistically inducing the expression of NFATc1, a master regulator of osteoclastogenesis (11). Although NFATc1 is known as an essential factor regulating osteoclast-specific gene expression programs (11, 12), NFATc1 deficiency affects only a subset of RANKL-regulated transcriptional programs (13), implicating the importance of other transcription factors in gene regulation during osteoclast differentiation. Recently, association of the comprehensive transcriptional factor network with molecular pathways in osteoclasts has gained much interest, and identification of new transcriptional pathways controlling osteoclastogenesis will offer promising therapeutic targets for the treatment of pathological bone disorders such as osteoporosis.

The importance of metabolic reprogramming in osteoclast differentiation is increasingly appreciated. Metabolic adaptation to meet increased energy demand is required to undergo osteoclast differentiation (7, 14–17). Recent studies have shown that several factors such as peroxisome proliferator–activated receptor γ coactivator 1β (PGC1β), PPARγ, and estrogen receptor–related receptor α (ERRα) govern key metabolic processes by transcriptionally regulating distinct metabolic genes during osteoclast differentiation as part of bone remodeling (18–21). However, whether there exists a key upstream regulator that controls these factors during RANKL-induced metabolic reprogramming is not clear.

In this study, we demonstrate that MYC and MYC-mediated regulation of oxidative respiration provide potential links between RANK signaling and metabolic reprogramming during
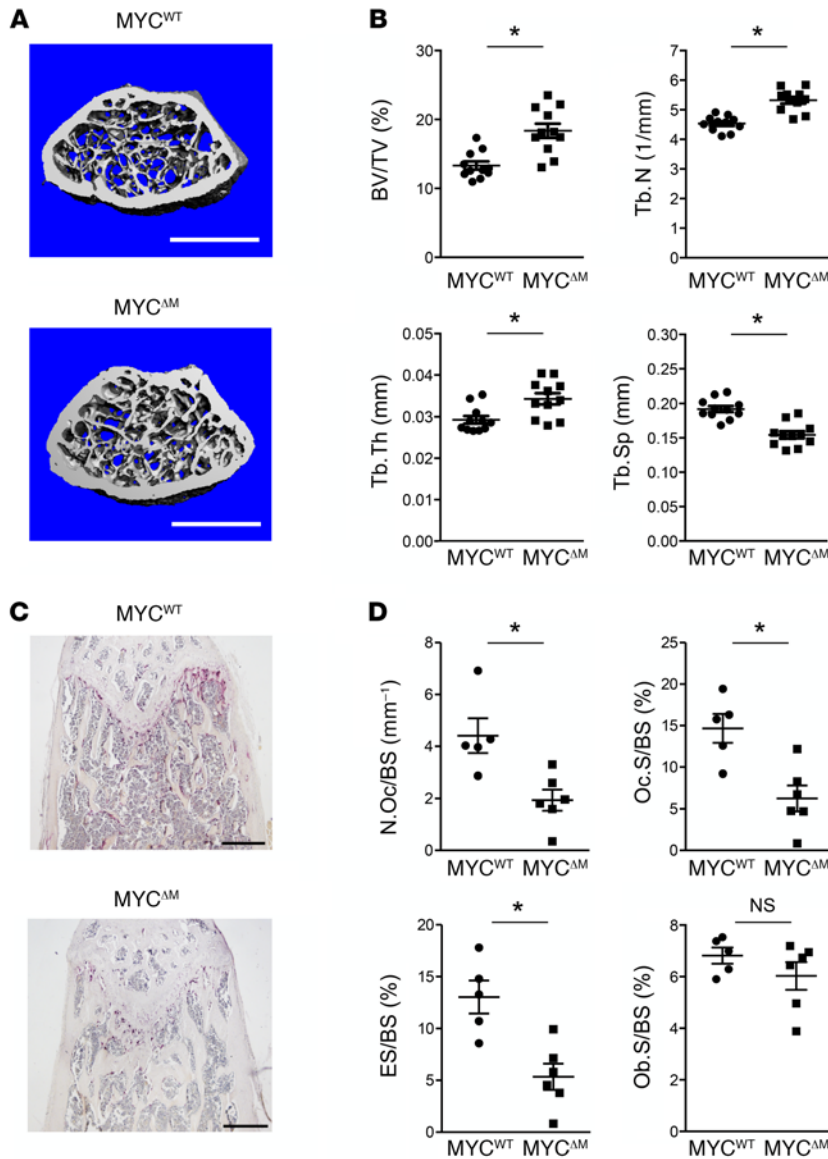
Figure 1. Myeloid-specific MYC-deficient mice have high bone mass. (**A** and **B**) μCT analysis of femurs from 12-week-old male MYC$^{\Delta M}$ and littermate control MYC^{WT} mice (*n* = 11 per group). (**A**) Representative images show trabecular architecture by μCT reconstruction in the distal femurs. Scale bars: 1 mm. (**B**) μCT measurements for the indicated parameters in distal femurs. Bone volume/tissue volume ratio (BV/TV), trabecular numbers (Tb.N), trabecular thickness (Tb.Th), and trabecular space (Tb.Sp) were determined by μCT analysis. (**C** and **D**) Histomorphometric analysis of femurs from 12-week-old male MYC$^{\Delta M}$ and MYC^{WT} mice (*n* ≥5). (**C**) Representative images showing TRAP-positive, multinucleated osteoclasts (red). Scale bars: 200 μm. (**D**) Plots show the number of osteoclasts per bone surface (N.Oc/BS), osteoclast surface area per bone surface (Oc.S/BS), eroded surface per bone surface (ES/BS), and osteoblast surface area per bone surface (Ob.S/BS). All data are shown as the mean ± SEM. *P < 0.05, by 2-tailed, unpaired *t* test in **B** and **D**.

osteoclastogenesis and identify a MYC/ERRα pathway that drives metabolic reprogramming during osteoclast differentiation as an important regulator of physiological and pathological bone loss. Moreover, our study highlights the possibility that pharmacological inhibition of ERRα may offer translational potential for the treatment of human bone disorders such as osteoporosis.

Results

Myeloid-specific deletion of MYC causes increased bone mass and decreased osteoclastogenesis. MYC was transiently expressed in the early stage of osteoclastogenesis (within 24 hours after RANKL stimulation) in both human and mouse osteoclast precursors (OCPs) (Supplemental Figure 1; supplemental material available online with this article; https://doi.org/10.1172/JCI89935DS1). To determine the role of this transient MYC expression in OCPs in physiological bone remodeling, we first investigated the bone phenotype of *Myc* conditional knockout mice generated by crossing *Myc*$^{fl/fl}$ mice with *LysM-Cre* mice (22) to specifically delete *Myc* in myeloid/osteoclast lineage cells (hereafter referred to as MYC$^{\Delta M}$

mice). Microcomputed tomography (μCT) analysis of 12-week-old male and female MYC$^{\Delta M}$ mice clearly indicated increased bone mass compared with that seen in their littermate controls (*LysM-Cre*, hereafter referred to as MYC^{WT} mice) (Figure 1, A and B, and Supplemental Figure 2, A and B). The body weight was not affected by *Myc* deletion in either male or female mice (Supplemental Figure 2C). Bone histomorphometric analysis revealed significantly decreased trabecular osteoclast numbers and surface area as well as bone resorption activity (eroded surface area) in MYC$^{\Delta M}$ mice, whereas the osteoblast surface areas were comparable (Figure 1, C and D). These results suggest that the high-bone-mass phenotype of MYC$^{\Delta M}$ mice was caused by compromised osteoclast activity and that MYC plays an important role in physiological bone remodeling.

Next, we isolated OCPs from MYC$^{\Delta M}$ bone marrow and evaluated in vitro osteoclast differentiation in the presence of macrophage-CSF (M-CSF) and RANKL. MYC was efficiently diminished in MYC-deficient OCPs (Supplemental Figure 3). MYC deficiency resulted in essentially a complete failure of OCPs to differentiate
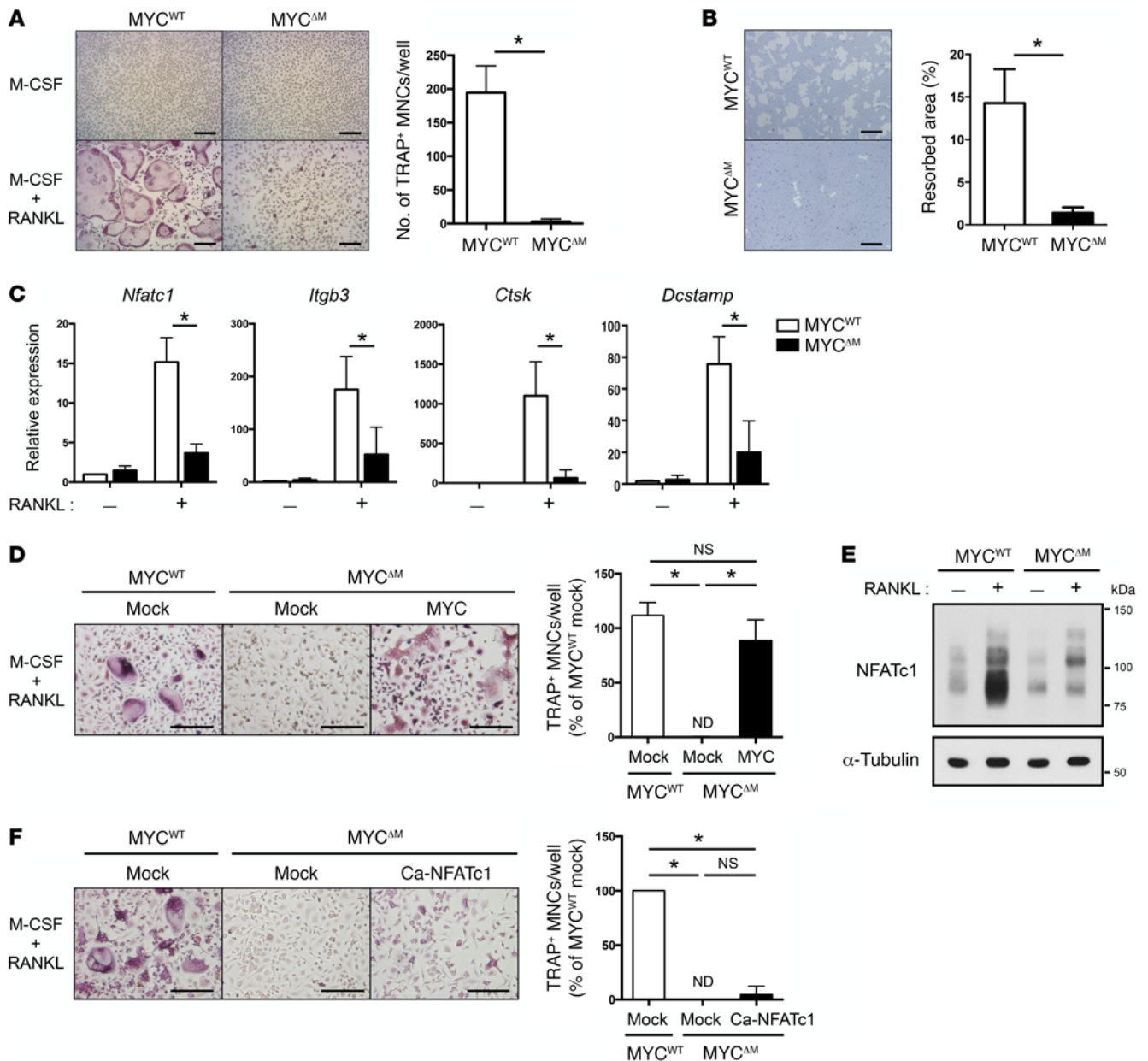
Figure 2. MYC is important for osteoclast differentiation and resorption. (**A**) Representative images show osteoclast differentiation in control (MYC^{WT}) and MYC-deficient (MYC$^{\Delta M}$) OCPs stimulated with RANKL (50 ng/ml). Scale bars: 200 μm. Graph depicts the number of TRAP-positive multinucleated cells (MNCs) counted in triplicate from 5 independent experiments. (**B**) Representative images show bone resorption activity of MYC^{WT} and MYC$^{\Delta M}$ OCPs stimulated with RANKL. Scale bars: 200 μm. Graph depicts the percentage of resorbed pit area per total area from at least 3 experiments. (**C**) Expression of osteoclast-related genes (relative to the *Hprt* housekeeping gene) on day 3 after RANKL stimulation (*n* = 8). (**D**) Osteoclast differentiation in mock-infected or MYC-transduced MYC-deficient OCPs stimulated with RANKL (50 ng/ml). Representative images of TRAP-stained cells are shown. Scale bars: 200 μm. Graph shows the number of TRAP-positive MNCs counted in triplicate from at least 4 experiments. (**E**) Immunoblot of whole-cell lysates using NFATc1 and α-tubulin antibodies. α-Tubulin served as a loading control. Data are representative of 3 experiments. (**F**) Osteoclast differentiation in mock-infected or Ca-NFATc1–transduced MYC-deficient OCPs. Representative images of TRAP-stained cells are shown. Scale bars: 200 μm. Graph shows the number of TRAP-positive MNCs counted in triplicate from at least 3 experiments. All data are shown as the mean ± SEM. *$P < 0.05$, by 2-tailed, unpaired *t* test (**A** and **B**); 2-way ANOVA with Tukey's post-hoc test (**C**); 1-way ANOVA with Tukey's post-hoc test (**D** and **F**). ND, not detected.

into multinucleated tartrate-resistant acid phosphatase–positive (TRAP-positive) cells that resorb bone (Figure 2, A and B). Accordingly, RANKL-induced expression of osteoclast marker genes such as *Itgb3* (encodes β3 integrin), *Ctsk* (encodes cathepsin K), and *Dcstamp* (encodes dendrocyte-expressed seven-transmembrane protein) was strongly suppressed in MYC-deficient OCPs (Figure

2C). Ectopic expression of MYC rescued the defect in osteoclastogenesis in MYC-deficient OCPs (Figure 2D), thus confirming that deletion of *Myc* is responsible for the loss of osteoclastogenesis. We initially reasoned that the complete loss of osteoclastogenesis could be explained by decreased bone marrow osteoclast progenitor cells in MYC$^{\Delta M}$ mice or their decreased proliferation in vitro.
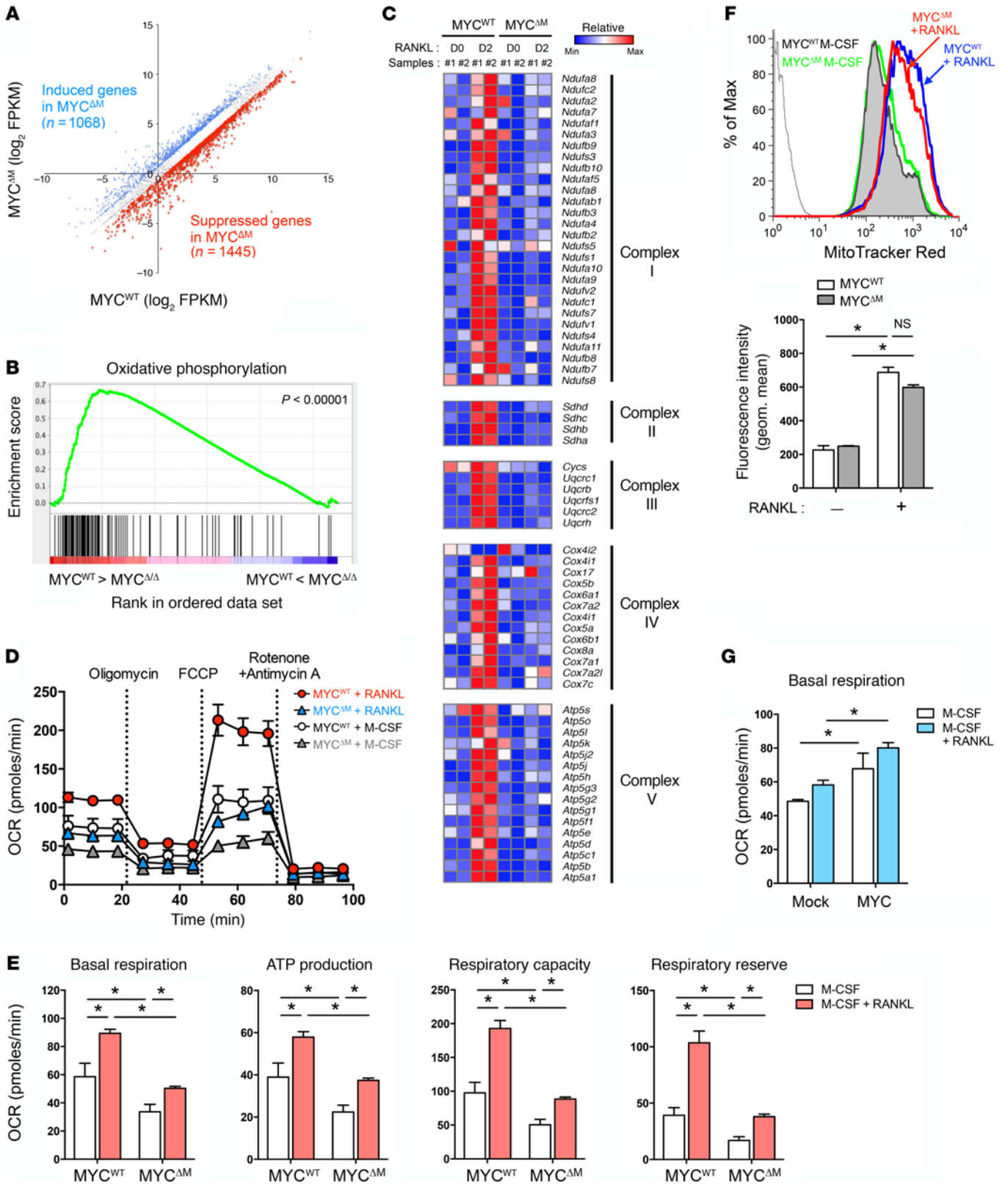
A

Induced genes
in MYC$^{\Delta M}$
($n = 1068$)

Suppressed genes
in MYC$^{\Delta M}$
($n = 1445$)

MYC$^{\Delta M}$ (log$_2$ FPKM)

MYC^{WT} (log$_2$ FPKM)

B

Oxidative phosphorylation

$P < 0.00001$

Enrichment score

MYC^{WT} > MYC$^{\Delta/\Delta}$ MYC^{WT} < MYC$^{\Delta/\Delta}$

Rank in ordered data set

C

MYC^{WT} MYC$^{\Delta M}$

RANKL :   D0   D2   D0   D2

Samples : #1 #2 #1 #2   #1 #2 #1 #2

Relative
Min   Max

Ndufa8
Ndufc2
Ndufa2
Ndufa7
Ndufaf1
Ndufa3
Ndufb9
Ndufs3
Ndufb10
Ndufa15
Ndufa8
Ndufab1
Ndufb3
Ndufa4
Ndufb2
Ndufs5   Complex
Ndufs1   I
Ndufa10
Ndufa9
Ndufv2
Ndufc1
Ndufs7
Ndufv1
Ndufs4
Ndufa11
Ndufb8
Ndufb7
Ndufs8

Sdhd
Sdhc   Complex
Sdhb   II
Sdha

Cycs
Uqcrc1
Uqcrb   Complex
Uqcrfs1   III
Uqcrc2
Uqcrh

Cox4i2
Cox4i1
Cox17
Cox5b
Cox6a1
Cox7a2
Cox4i1   Complex
Cox5a   IV
Cox6b1
Cox8a
Cox7a1
Cox7a2l
Cox7c

Atp5s
Atp5o
Atp5l
Atp5k
Atp5j2
Atp5j
Atp5h
Atp5g3
Atp5g2   Complex
Atp5g1   V
Atp5f1
Atp5e
Atp5d
Atp5c1
Atp5b
Atp5a1

D

Oligomycin   FCCP   Rotenone
+Antimycin A

OCR (pmoles/min)

● MYC^{WT} + RANKL
▲ MYC$^{\Delta M}$ + RANKL
○ MYC^{WT} + M-CSF
△ MYC$^{\Delta M}$ + M-CSF

Time (min)

F

MYC^{WT}M-CSF   MYC$^{\Delta M}$
+ RANKL

MYC$^{\Delta M}$ M-CSF   MYC^{WT}
+ RANKL

% of Max

MitoTracker Red

☐ MYC^{WT}
▨ MYC$^{\Delta M}$

*   NS
*

Fluorescence intensity
(geom. mean)

RANKL :   −   +

G

Basal respiration

☐ M-CSF
▨ M-CSF
+ RANKL

*
*

OCR (pmoles/min)

Mock   MYC

E

Basal respiration

OCR (pmoles/min)

*
*   *

MYC^{WT} MYC$^{\Delta M}$

ATP production

*
*   *

MYC^{WT} MYC$^{\Delta M}$

Respiratory capacity

*
*   *

MYC^{WT} MYC$^{\Delta M}$

Respiratory reserve

*
*   *

☐ M-CSF
▨ M-CSF + RANKL

MYC^{WT} MYC$^{\Delta M}$

Figure 3. MYC deficiency impairs mitochondrial respiration during osteoclast differentiation. Control (MYC^{WT}) and MYC-deficient (MYC$^{\Delta M}$) OCPs were stimulated with RANKL (50 ng/ml) for 2 days. (**A**) Scatterplot of global gene expression profiles of MYC^{WT} and MYC$^{\Delta M}$ OCPs derived from RNA-seq analysis. (**B**) GSEA of RANKL-stimulated MYC$^{\Delta M}$ OCPs, with genes ranked on the basis of expression in MYC$^{\Delta M}$ OCPs relative to that in MYC^{WT} OCPs, showing the distribution of genes in the oxidative phosphorylation gene set against the ranked list of the genes from the RNA-seq analysis. (**C**) Heatmap of RNA-seq FPKM values for genes involved in oxidative phosphorylation in MYC^{WT} and MYC$^{\Delta M}$ OCPs following RANKL stimulation for 2 days. RNA-seq data from 2 biological replicates were used. D0, day 0 without RANKL stimulation; D2, day 2 following RANKL stimulation; Min, minimum; Max, maximum. (**D** and **E**) Mitochondrial function was assessed by real-time OCR measurement after sequential treatment of compounds modulating mitochondrial function. The OCR was normalized to the relative amount of DNA. (**D**) Representative time course data. (**E**) Assessment of mitochondrial activity as described in Supplemental Figure 9 ($n = 3$). (**F**) Measurements of mitochondrial mass using MitoTracker Red with flow cytometry ($n = 3$). (**G**) The basal OCR was measured with mock-infected or MYC-transduced MYC-deficient OCPs stimulated with RANKL (50 ng/ml) for 2 days ($n = 3$). All data are shown as the mean ± SEM. *$P < 0.05$, by 2-way ANOVA with Tukey's post-hoc test.

However, consistent with a previous report showing intact bone marrow and lymphoid compartments in *Myc*-knockout mice (23), the total number and frequency of the CD11b$^{-/lo}$Ly6C^{hi} osteoclast progenitor population (24) residing in the bone marrow were comparable between MYC$^{\Delta M}$ and MYC^{WT} mice (Supplemental Figure 4, A and B). In addition, MYC deficiency had modest effects on apoptosis, and MYC-deficient OCPs showed decreased proliferation. These results could not explain the striking effects of MYC deficiency on osteoclastogenesis (Supplemental Figure 4, C and D). Furthermore, RANK expression and proximal RANKL signaling were not altered in MYC-deficient OCPs (Supplemental Figure 5). Taken together, these results indicate that RANKL-inducible MYC is crucial for osteoclast differentiation in vitro.

MYC is a crucial regulator of oxidative metabolism during osteoclastogenesis. Consistent with our previous results showing MYC as a direct regulator of NFATc1 (8), expression levels of both NFATc1 mRNA and protein were suppressed in MYC-deficient OCPs (Figure 2, C and E). We first reasoned that restoration of NFATc1 activity would compensate for impaired osteoclastogenesis in MYC-deficient OCPs. To test this notion, we transduced MYC-deficient OCPs with a retrovirus encoding the constitutively active form of NFATc1 (Ca-NFATc1). With RANKL stimulation, the expression of NFATc1 and β3 integrin, a downstream target of NFATc1 (12), in Ca-NFATc1–transduced MYC-deficient OCPs was comparable to that in control OCPs (Supplemental Figure 6), but was not sufficient to rescue the defective osteoclastogenesis seen in MYC-deficient OCPs (Figure 2F), suggesting that MYC regulates alternative pathways that are required to cooperate with NFATc1 to promote osteoclastogenesis.

To find new pathways and mechanisms regulated by MYC during osteoclastogenesis, we performed an unbiased transcriptomic analysis using high-throughput RNA sequencing (RNA-seq) with 2 biological replicates after stimulating cells with RANKL for 2 days (Supplemental Figure 7). A total of 1,068 genes were induced (>1.5 fold) and 1,445 genes were suppressed (>1.5 fold) in MYC-deficient OCPs compared with control OCPs (Figure 3A). We used gene set enrichment analysis (GSEA) (25) to broadly test for enrichment of well-defined gene sets from the comprehensive

Molecular Signature Data Base (MSigDB), version 5.1 (www.broadinstitute.org) and Ingenuity Pathway Analysis (IPA) for MYC-dependent genes, which are downregulated in MYC$^{\Delta M}$ OCPs relative to MYC^{WT} OCPs on day 2 after RANKL stimulation. Genes associated with metabolic pathways, including oxidative phosphorylation and the TCA cycle, were significantly enriched in MYC-dependent genes (Table 1, Figure 3B, and Supplemental Figure 8). Accordingly, metabolic genes involved in oxidative phosphorylation, which are highly induced in MYC^{WT} OCPs upon RANKL stimulation, were suppressed in MYC$^{\Delta M}$ OCPs (Figure 3C).

Recent studies show that a metabolic shift toward oxidative processes during osteoclast differentiation provides metabolites (15–17), although key upstream modulators that induce oxidative metabolic reprogramming in osteoclastogenesis are not yet clarified. To directly test whether MYC mediates the RANKL-induced shift toward mitochondrial respiration, we performed an extracellular flux analysis 2 days after RANKL stimulation (Figure 3, D and E, and Supplemental Figure 9). RANKL stimulation led to a characteristic increase in the basal oxygen consumption rate (OCR) in control OCPs (Figure 3, D and E). Strikingly, the basal OCR and other mitochondrial activities such as ATP production, respiratory capacity (maximal electron transport chain activity), and respiratory reserve (flexibility with increased energy demand) were severely impaired in MYC-deficient OCPs upon RANKL stimulation (Figure 3, D and E). We confirmed that the RANKL-induced increase in mitochondrial mass was comparable between MYC-deficient and control OCPs (Figure 3F), indicating that the impaired mitochondrial respiration in MYC-deficient OCPs was not caused by a defect in the quantity of mitochondria. Moreover, the basal OCR was greatly increased by the ectopic expression of MYC (Figure 3G). Consistent with previous reports (7, 16), perturbation of metabolic pathways such as glutaminolysis, glycolysis, and oxidative phosphorylation using specific inhibitors severely abrogated osteoclast differentiation (Supplemental Figure 10), implicating the significance of metabolic reprogramming in osteoclastogenesis. Collectively, these results indicate that MYC is a crucial regulator of RANKL-activated mitochondrial respiration that supports an increased energy demand during osteoclast differentiation.

MYC regulates ERRα during osteoclast differentiation. MYC expression is kept at low levels in normal cells via accelerated decay mechanisms, and aberrant expression of MYC causes tumorigenesis (5). In osteoclastogenesis, MYC expression is transient (Supplemental Figure 1), and thus we hypothesized that MYC induces downstream transcription factors to directly activate osteoclast-related genes and sustain osteoclast differentiation. To discover these factors, we used GSEA to identify transcription factor–binding motifs that are enriched in the promoters of MYC-dependent genes, which can be regulated directly by MYC, or indirectly via MYC-induced transcription factors. In addition to recovering the MYC-binding motif, which validated the approach, and the NFAT-binding motif, as expected on the basis of our previous work (8), we found highly significant enrichment of binding motifs for Sp1 transcription factor (SP1), estrogen-related receptor (ERR), MYC-associated zinc finger protein (MAZ), and splicing factor 1 (SF1) (Table 2); of these, only estrogen-related receptor α (*Esrra*, encoding ERRα) was dynamically regulated during osteoclast differentiation (Figure 4A).

Table 1. Gene ontology analysis of MYC^WT and MYC^ΔM OCPs derived from RNA-seq analysis

Gene set	P value
Suppressed genes in MYC^ΔM OCPs	
KEGG_Ribosome	9.73×10^{-91}
KEGG_Oxidative phosphorylation	1.54×10^{-45}
KEGG_Parkinsons disease	3.21×10^{-39}
KEGG_Alzheimers disease	2.28×10^{-30}
KEGG_Citrate cycle TCA cycle	4.52×10^{-10}
Induced genes in MYC^ΔM OCPs	
KEGG_MAPK signaling pathway	2.75×10^{-16}
KEGG_Pathways in cancer	2.94×10^{-12}
KEGG_Chemokine signaling	2.45×10^{-11}
KEGG_B cell receptor signaling	1.72×10^{-10}
KEGG_Focal adhesion	2.74×10^{-10}

KEGG, Kyoto Encyclopedia of Genes and Genomes.

ERRα is not an estrogen receptor, but instead is a nuclear receptor implicated in increasing cellular energy metabolism in tissues such as liver and skeletal muscle in response to environmental challenges that require high energy levels (26–28). Although ERRα has been implicated in osteoclastogenesis (26, 27), a role for ERRα in mediating the effects of MYC on cell phenotype and metabolism has not been previously appreciated, and mechanisms by which ERRα promotes osteoclastogenesis are mostly unknown. We directly tested the role of MYC in inducing expression of *Esrra*, which encodes ERRα. Induction of ERRα by RANKL (Figure 4, B and C, and Supplemental Figure 11, A and B) was abrogated in both mouse and human MYC-deficient OCPs (Figure 4, B and C, and Supplemental Figure 11C). Of note, MYC-deficient human OCPs had impaired osteoclastogenesis (Supplemental Figure 11D). Compromised ERRα expression in MYC-deficient OCPs was restored by the reintroduction of MYC using retroviral transduction (Figure 4D), indicating that the expression of ERRα is dependent on MYC. In contrast, the expression of PGC1β, a well-known ERRα coactivator, was not altered by the overexpression of MYC (Figure 4D), and MYC deficiency marginally decreased PGC1β expression (Figure 4C). RANKL-induced expression of ERRα target genes was strongly attenuated in MYC-deficient OCPs (Supplemental Figure 12A). ChIP assays showed that RANKL induced the recruitment of MYC to the *Esrra* promoter (Supplemental Figure 12B) and that *Esrra* promoter activity was dependent on MYC (Supplemental Figure 12C). Taken together, these results show that MYC directly regulates ERRα in osteoclasts.

The MYC/ERRα axis regulates mitochondrial respiration in osteoclastogenesis. Consistent with previous reports using genetic approaches (19, 21), ERRα deficiency and treatment with XCT790 (29), an ERRα inhibitor, suppressed RANKL-induced osteoclast differentiation (Supplemental Figure 13 and Supplemental Figure 14A). Importantly, forced MYC expression, which restored osteoclast differentiation in MYC-deficient OCPs (Figure 2D and Figure 5A, left panels), was not able to restore osteoclast differentiation when ERRα was inhibited by XCT790 (Figure 5A). Taken

together, these results identify a link between MYC and ERRα in osteoclasts and establish that ERRα is required for the effects of MYC on osteoclastogenesis.

ERRα transcriptionally regulates the expression of genes encoding energy metabolism regulators (28, 30, 31). To test whether ERRα could functionally phenocopy the role of MYC in mitochondrial respiration in osteoclasts, we measured mitochondrial respiration following RANKL stimulation using ERRα-deficient OCPs isolated from ERRα-null mice. Indeed, ERRα-deficient OCPs had a diminished RANKL-induced basal OCR and other mitochondrial activities (Figure 5, B and C). Consistently, expression of RANKL-inducible genes involving oxidative phosphorylation was significantly abrogated in ERRα-deficient or XCT790-treated OCPs (Figure 5D). These results strongly support a role for a novel MYC/ERRα pathway in RANKL-activated mitochondrial respiration.

We next investigated whether overexpression of ERRα could restore impaired osteoclastogenesis in MYC-deficient OCPs. MYC-deficient OCPs were transduced with a retrovirus encoding ERRα-turboGFP (ERRα-tGFP), and the expression of ERRα-tG-FP was analyzed by immunoblotting (Supplemental Figure 15B). Ectopic expression of ERRα had a minimal effect on osteoclastogenesis in MYC-deficient OCPs (Supplemental Figure 15), which was similar to the inability of NFATc1 alone to rescue osteoclastogenesis in MYC-deficient OCPs (Figure 2F). Although ERRα-deficient osteoclasts completely failed to resorb bone (Supplemental Figure 14B), RANKL-induced expression of NFATc1 and β3 integrin in ERRα-deficient osteoclasts was comparable to that in WT osteoclasts (Supplemental Figure 14C), supporting the notion that ERRα is not necessary for NFATc1 expression. Therefore, we tested whether both NFATc1 and ERRα are required for MYC-mediated osteoclastogenesis. Indeed, coexpression of Ca-NFATc1 and ERRα was able to partly rescue the impaired osteoclastogenesis in MYC-deficient OCPs (Figure 5E and Supplemental Figure 16). Collectively, our results suggest that ERRα and NFATc1 regulate distinct aspects of osteoclast differentiation and need to cooperate for effective osteoclastogenesis.

Targeting of the MYC/ERRα pathway protects mice against pathological bone loss. To test the importance of the MYC/ERRα pathway in pathological bone resorption and the efficacy of therapeutic targeting of this pathway to prevent bone loss for translational implications, we used the ovariectomy (OVX) model of estrogen

Table 2. Motif analysis with GSEA using MYC-dependent genes on day 2 after RANKL stimulation

Transcription factor	Binding motif	P value
SP1	GGGCGGR	3.71×10^{-34}
ERR	TGACCTY	7.9×10^{-27}
MAZ	GGGAGGRR	3.54×10^{-19}
SF1	TGACCTTG	1.19×10^{-18}
NFAT	TGGAAA	1.28×10^{-16}
MYC	CACGTG	6.19×10^{-14}

The 5 most enriched transcription factor–binding motifs in a ±2-kb region of the transcriptional start site in MYC-dependent, RANKL-inducible genes ($P < 10^{-14}$).
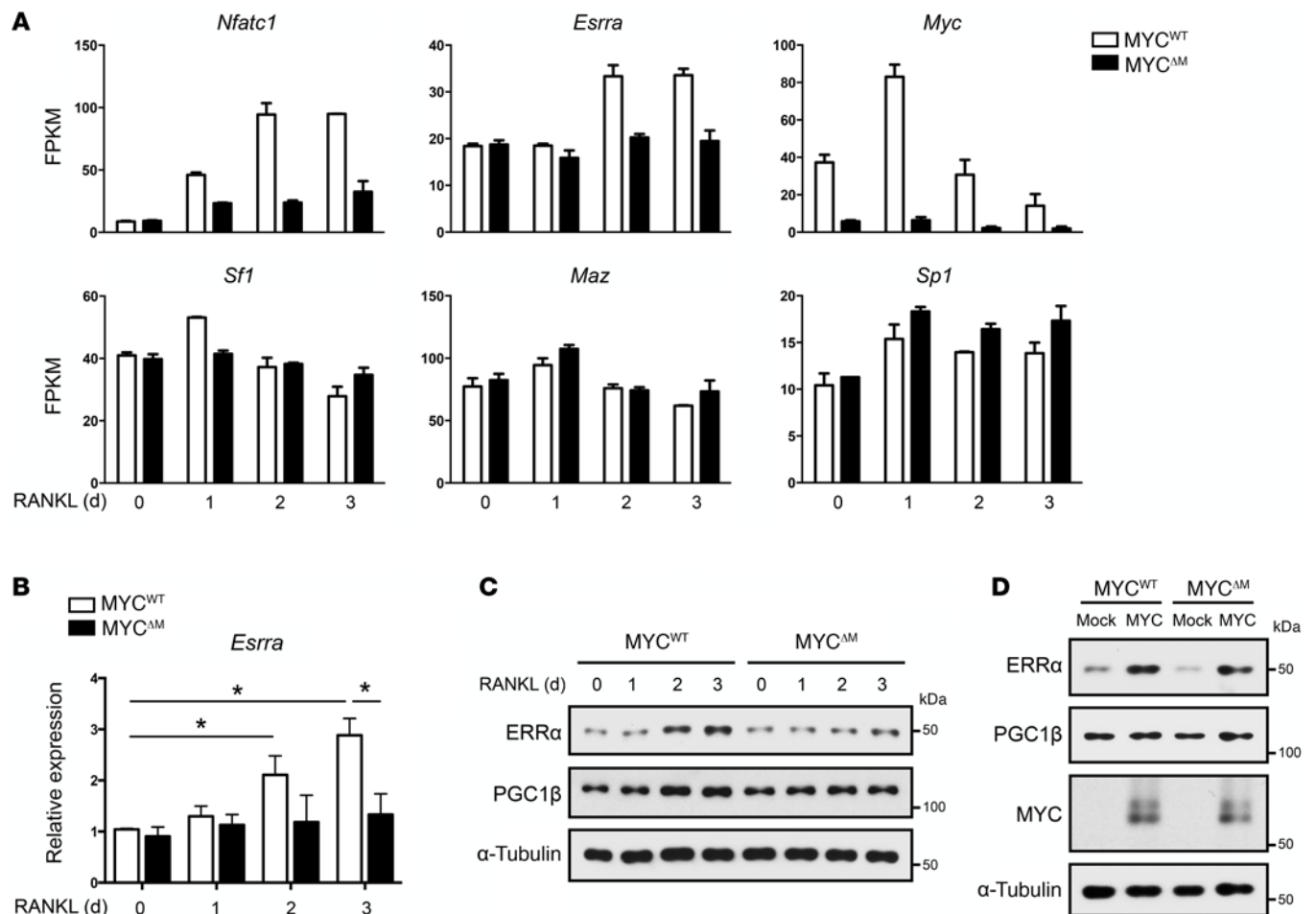
Figure 4. MYC regulates ERRα expression in osteoclastogenesis. (**A**) RNA-seq FPKM values for *Nfatc1*, *Esrra*, *Myc*, *Sf1*, *Maz*, and *Sp1* in control (MYC^WT) and MYC-deficient (MYC^ΔM) OCPs during osteoclast differentiation. RNA-seq data from 2 biological replicates are shown, and the level of each gene expression in each sample was normalized by means of FPKM. Data are shown as the mean ± SEM. (**B** and **C**) Expression of ERRα in MYC^WT and MYC^ΔM OCPs during osteoclastogenesis. (**B**) mRNA expression of *Esrra* (relative to the *Hprt* housekeeping gene), as measured by real-time quantitative PCR ($n = 6$). Data are shown as the mean ± SEM. $*P < 0.05$, by 2-way ANOVA with Tukey's post-hoc test. (**C**) Protein expression of ERRα and PGC1β, as determined by immunoblotting. Data are representative of 3 experiments. (**D**) Effect of MYC overexpression on ERRα and PGC1β expression levels. Protein expression of ERRα in mock-infected or MYC-transduced cells was determined by immunoblotting. Data are representative of 3 experiments.

deficiency–mediated bone loss (Figure 6A). Strikingly, μCT analysis revealed that MYC^ΔM mice were almost completely protected against OVX-induced bone loss, whereas MYC^WT mice showed significant bone loss 6 weeks after OVX (Figure 6, B and C). Bone histomorphometric analysis also revealed a significant decrease in osteoclast numbers in MYC^ΔM OVX mice compared with numbers in MYC^WT OVX mice (Figure 6D). These results suggest that MYC in osteoclasts plays a crucial role in pathological bone resorption and that MYC is a potential therapeutic target for osteoporosis.

However, given the inherent structure of MYC, it is difficult to design a small-molecule inhibitor that directly binds to MYC (32, 33). Thus, we hypothesized that inhibiting downstream effector molecules such as ERRα would be an alternative method for suppressing MYC function. To test whether inhibition of ERRα shows a similar therapeutic efficacy in the treatment of pathological bone loss, we treated OVX mice with XCT790, a small-molecule inhibitor of ERRα, in the OVX osteoporosis model using a therapeutic experimental design. XCT790 treatment was started

3 weeks after OVX and continued for 6 weeks (Figure 7A). To test the efficacy of XCT790 on osteoporosis, we used two different mouse strains with different basal bone density, one with high basal bone mass (26.12% ± 5.12%; Figure 7, C and D) and the other with low basal bone mass (13.30% ± 2.66%; Figure 7, D and E), to account for strain-to-strain variations. XCT790 treatment significantly protected both strains of mice from OVX-induced bone loss (Figure 7, B–E), although the effect of XCT790 was milder than that seen with MYC deficiency. In addition, XCT790 treatment in sham-operated mice had a marginal effect on in vivo bone phenotype and formation, as measured by bone volume, bone formation rate (BFR), and mineral apposition rate (MAR) (Supplemental Figure 17, A–D). Consistently, we also found that XCT790 did not enhance in vitro osteoblastogenesis or activity at the dosage that suppressed osteoclastogenesis (Supplemental Figure 17, E–H). The expression of Runt-related transcription factor 2 (*Runx2*) was comparable between XCT790- and vehicle-treated cells (Supplemental Figure 17I). Taken together, these results suggest that
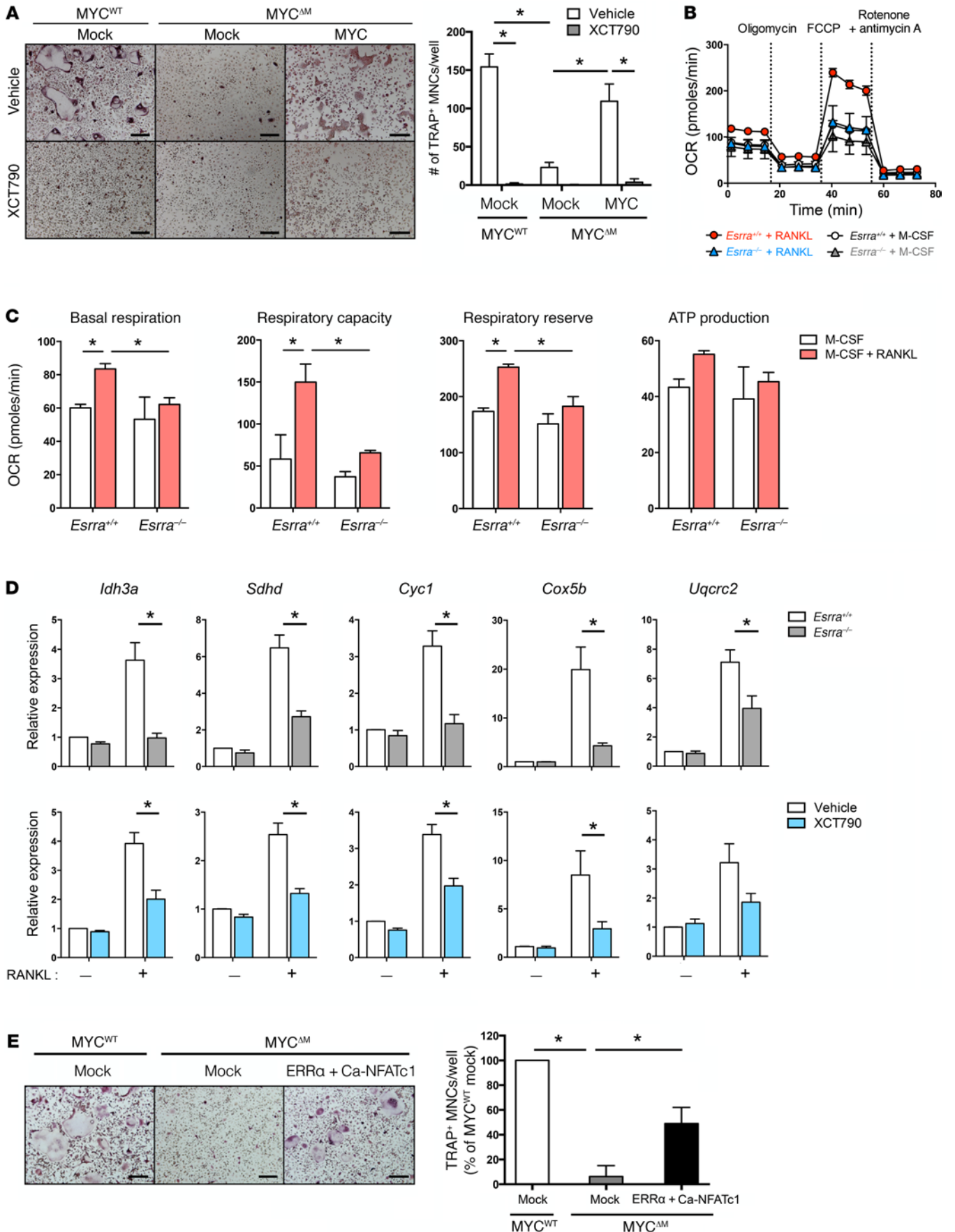
Figure 5. MYC-dependent expression of ERRα is required for osteoclastogenesis. (**A**) Osteoclast differentiation in mock-infected or MYC-transduced MYC^ΔM OCPs treated with XCT790 (10 μM). Representative images of TRAP-stained cells are shown. Scale bars: 200 μm. Graph indicates the number of TRAP-positive MNCs counted in triplicate from at least 3 experiments. (**B** and **C**) Effect of ERRα deficiency on mitochondrial respiration. Control (*Esrra^+/+*) and ERRα-deficient (*Esrra^−/−*) OCPs were stimulated with RANKL (50 ng/ml) for 2 days, and then the mitochondrial respiration rate of those cells was assessed by real-time measurement of the OCR (*n* = 4). (**B**) Representative time course data. (**C**) Assessment of mitochondrial activity as described in Supplemental Figure 9. (**D**) mRNA expression of oxidative phosphorylation–related genes in *Esrra^+/+*^ and *Esrra^−/−*^ OCPs and XCT790-treated OCPs (10 μM) following RANKL stimulation (*n* = 3). *Idh3a*, isocitrate dehydrogenase 3; *Sdhd*, succinate dehydrogenase complex, subunit D, integral membrane protein; *Cyc1*, cytochrome c-1; *Cox5b*, cytochrome c oxidase subunit Vb; *Uqcrc2*, ubiquinol cytochrome c reductase core protein 2. (**E**) Osteoclast differentiation in mock-infected or Ca-NFATc1– and ERRα-transduced MYC^ΔM OCPs. Representative images of TRAP-stained cells are shown. Scale bars: 200 μm. Graph shows the number of TRAP-positive MNCs counted in triplicate from 4 independent experiments. All data are shown as the mean ± SEM. *$P < 0.05$, by 2-way ANOVA with Tukey's post-hoc test (**A**, **C**, and **D**) and 1-way ANOVA with Tukey's post-hoc test (**E**).

inhibition of the MYC/ERRα pathway holds promise for the treatment of bone resorption, especially in conditions associated with increased MYC expression in OCPs.

Discussion

Constraining accelerated bone-resorbing osteoclast differentiation is an effective strategy for the treatment of osteoporosis (34–37). Our study highlights the importance of MYC in physiological and pathological bone remodeling and identifies a MYC/ERRα pathway as an important regulator of oxidative metabolism in osteoclasts. Moreover, targeting ERRα by XCT790 attenuated OVX-induced bone loss, an established model for human osteoporosis. These findings highlight the importance of the MYC/ERRα pathway as a potential therapeutic target with translational potential to treat pathological bone resorption.

It is generally accepted that MYC plays an essential role in metabolic mechanisms. Our study shows that MYC is a key determinant of metabolic reprogramming in osteoclasts. Recent studies focused on the role of MYC in metabolism reveal that MYC regulates activation-induced glycolysis and glutaminolysis in T cells (38), and inhibition of MYC-MAX interaction suppresses glutamine metabolism in in vitro osteoclastogenesis (7). However, how MYC integrates anabolic metabolism into different cellular functions in a cell type–specific manner is not clear. Our work demonstrates how alteration of metabolic pathways by MYC impacts physiological and pathological bone resorption by osteoclasts. Therefore, our results provide new insights into the role of MYC in metabolic reprogramming during osteoclastogenesis, which has been less studied.

Understanding the molecular determinants of metabolic reprogramming in osteoclasts is important, but the metabolic regulation in osteoclast differentiation is not completely elucidated. Recent studies have shown that effective osteoclastogenesis requires metabolic regulation including glycolytic flux and oxidative phosphorylation (7, 14). Our study adds another layer of complexity in metabolic reprogramming by demonstrat-

ing the essential role of MYC in meeting energy and anabolic demands during osteoclast differentiation. In previous studies, increased oxidative phosphorylation has been partially mediated by increased mitochondrial biogenesis orchestrated by PGC1β (18) and is accompanied by an increase in S-adenosylmethionine (SAM) production (16). We have observed that the effect of MYC on oxidative phosphorylation is independent of mitochondrial biogenesis and that the overexpression of MYC is unable to regulate PGC1β expression, which suggests the uncoupling of PGC1β from oxidative phosphorylation in osteoclastogenesis. Supporting our observation, a recent study has also shown that the alternative NF-κB pathway induced by RANKL regulates osteoclastogenesis independently of mitochondrial biogenesis (17) and that PGC1β-deficient mice have a normal bone phenotype (19). Taken together, these results suggest that mitochondrial biogenesis is not a prerequisite for osteoclast formation and function.

Furthermore, our data establish MYC as a central regulator of oxidative metabolism in osteoclasts and place MYC at an upstream node in RANKL-induced osteoclastogenic signaling, where it is required for NFATc1 induction and the induction of respiratory metabolism mediated, in part, by ERRα. Although the coexpression of NFATc1 and ERRα substantially rescued defective osteoclastogenesis in MYC-deficient OCPs, the incomplete restoration suggests that additional pathways downstream of MYC may play a role in osteoclastogenesis. Our GSEA pathway analysis further revealed that MYC is involved in other processes such as the TCA cycle, but its role in the TCA cycle in osteoclasts is poorly defined. Thus, several pathways regulated by MYC in osteoclasts are likely to exist, and further studies to fully reveal the role of MYC in osteoclasts will be necessary.

Our transcriptional data reveal that MYC regulates metabolic pathways through its downstream target, ERRα, during osteoclastogenesis. ERRα has been shown to be important for osteoclastogenesis (19, 21), but the exact mechanism by which ERRα regulates osteoclast differentiation has remained unknown. We have shown, for the first time to our knowledge, a tight association between oxidative phosphorylation and the MYC/ERRα pathway during osteoclastogenesis. Emerging evidence has indicated that the induction of anabolic metabolic pathways by RANKL is important for osteoclastogenesis (7, 14–17), but the mechanisms by which these pathways are induced and their relationship to the NFATc1 program have not been clearly identified. We determined that ERRα deficiency results not only in defective oxidative phosphorylation but also in compromised bone resorption, without affecting RANKL-induced NFATc1 expression. In addition, either ERRα alone or NFATc1 alone did not rescue the impaired osteoclastogenesis seen in MYC-deficient OCPs. Although the importance of RANKL-induced NFATc1 as a master regulator of osteoclastogenesis is well established (11), our data suggest that the MYC/ERRα pathway described here is independent of, and works together with, NFATc1 to drive osteoclastogenesis.

Additionally, the deficiency of MYC in osteoclasts completely abrogates in vitro osteoclastogenesis and significantly protects mice against OVX-induced bone loss in vivo. Our results show that bone mass in MYC^ΔM mice was significantly increased (37%) compared with that of control mice at 12 weeks. However, despite the substantial decrease in the number of osteoclasts, aging com-
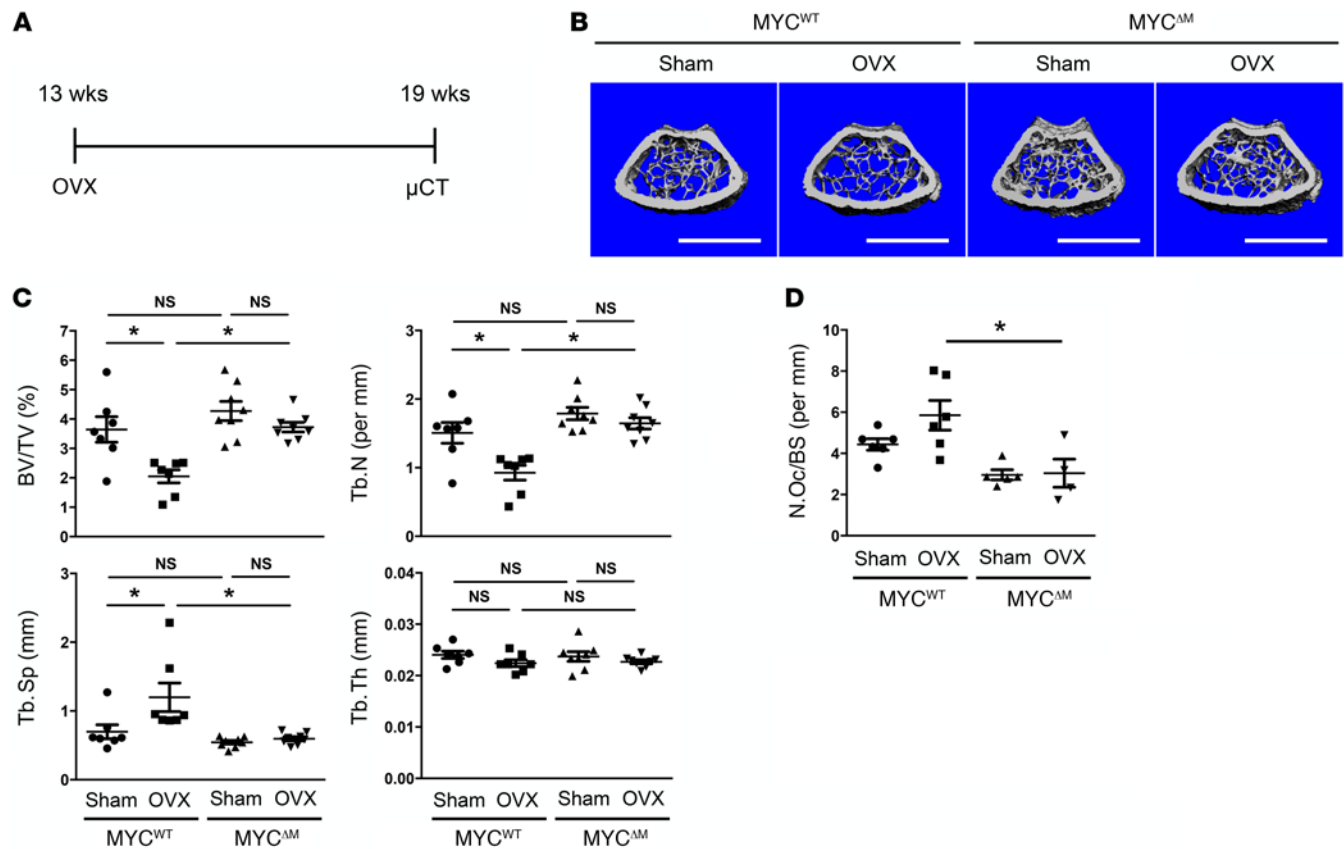
Figure 6. Ablation of MYC protects mice from OVX-induced pathological bone loss. (**A**) Schematic diagram illustrating the experimental design. (**B** and **C**) μCT analysis of femurs from 19-week-old sham-operated or OVX myeloid-specific MYC-deficient mice (MYC^ΔM) and control mice (MYC^WT). $n = 7$ sham-operated or OVX MYC^WT; $n = 8$ sham-operated or OVX MYC^ΔM mice. (**B**) Representative images show trabecular architecture by μCT reconstruction in distal femurs. Scale bars: 1 mm. (**C**) μCT measurements for the indicated parameters in distal femurs. Bone volume, trabecular numbers, trabecular thickness, and trabecular space were determined by μCT analysis. (**D**) Osteoclast numbers per bone surface were measured by histomorphometric analysis ($n ≥ 4$). All data are shown as the mean ± SEM. *$P < 0.05$, by 1-way ANOVA with Tukey's post-hoc test.

pensated for the difference in bone mass between the 2 groups. The discrepancy between in vivo and in vitro osteoclastogenesis has also been observed in many studies, including the studies in NF-κB–inducing kinase-deficient (NIK-deficient) and RelB proto-oncogene, NF-κB subunit–deficient (RelB-deficient) mice (17, 39). The absence of NIK or RelB in osteoclasts completely suppresses in vitro osteoclastogenesis and pathological osteolysis in the context of inflammation and bone metastasis, but has a minimal effect on basal bone phenotype (40, 41). Our study suggests that MYC may play a more prominent role in pathological conditions with accelerated bone loss such as osteoporosis than in physiological bone remodeling and that additional signals could compensate for impaired osteoclast activity in MYC^ΔM mice in vivo.

Our in vitro results from human blood–derived OCPs recapitulate our observations in murine OCPs, in that both showed the important role of MYC in osteoclasts, although the pattern of MYC expression or alteration of metabolic mechanisms in hyperactive osteoclasts during the pathogenesis of human osteoporosis is not known. Pathological conditions associated with excessive bone destruction include many diseases such as osteoporosis, rheumatoid arthritis, cancer metastases, and periprosthetic osteolysis. However, the known and druggable molecular targets in osteo-

clasts are limited, impeding the development of antiresorptive drugs with effective pipelines. We propose that, although MYC is considered undruggable, directly targeting signaling components downstream of MYC can be a strategy to block MYC functions in osteoclasts. ERRα is one of the downstream candidates of MYC, and its inhibitor, XCT790, suppresses osteoclastogenesis and bone loss in the murine post-OVX model of human osteoporosis. While ERRα is important for osteoclast differentiation and activity, ERRα deficiency has been shown to promote bone formation in vivo (42, 43). However, in our study, treatment with XCT790 showed a lack of enhancement of osteoblast function in vivo. The difference between our results and those from ERRα-null mice may be explained by the pharmacokinetics and efficiency of XCT790 or by the differences in dosing. Targeting of ERRα by specific small-molecule inhibitors that have an optimal therapeutic window and can suppress excessive bone resorption and promote bone formation may have beneficial effects on pathological bone loss.

In summary, we have identified MYC as a key upstream regulator of RANKL-induced metabolic reprogramming and demonstrated the importance of the MYC/ERRα axis in osteoclasts as an integrator of metabolic reprogramming to promote osteoclast differentiation in physiological and pathological bone resorption,
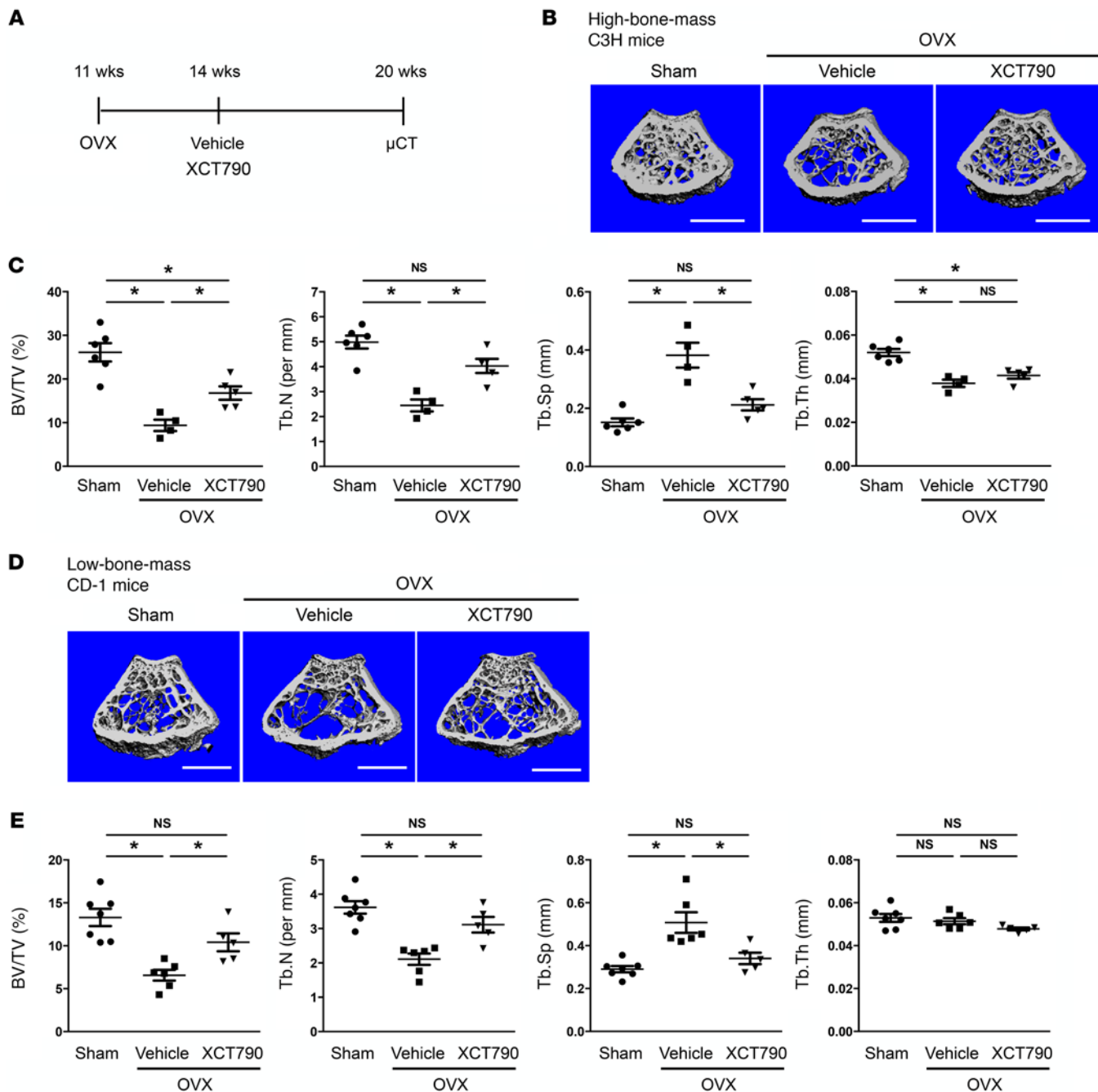
Figure 7. Therapeutic effect of XCT790 on the osteoporosis model. (**A**) Schematic diagram illustrating the experimental design. (**B** and **C**) μCT analysis of the femurs of sham-operated, vehicle-treated (sham, *n* = 6), vehicle-treated OVX (vehicle, *n* = 4), and XCT790-treated OVX (XCT790, *n* = 5) high-bone-mass C3H mice. (**B**) Representative images showing trabecular architecture by μCT reconstruction in the distal femurs of C3H mice. Scale bars: 1 mm. (**C**) μCT measurements for the indicated parameters in distal femurs. (**D** and **E**) μCT analysis of the femurs of sham-operated, vehicle-treated (sham, *n* = 7), vehicle-treated OVX (vehicle, *n* = 6), and XCT790-treated OVX (XCT790, *n* = 5) low-bone-mass CD-1 mice. (**D**) Representative images show trabecular architecture by μCT reconstruction in distal femurs. Scale bars: 1 mm. (**E**) μCT measurements for the indicated parameters in distal femurs. All data are shown as the mean ± SEM. *P < 0.05, by 1-way ANOVA with Tukey's post-hoc test.

opening up new lines of investigation to develop novel therapeutic interventions for pathological bone resorption.

Methods

Mice. All animals were maintained in a pathogen-free environment and were monitored by the investigators and staff at the Research Animal Resource Center of the Weill Cornell Medical College. All animals were randomly assigned to experimental groups. We generated MYC$^{\Delta M}$ mice by crossing *Myc$^{fl/fl}$* mice (The Jackson Laboratory) with *LysM-Cre* (MYC^{WT}) mice (The Jackson Laboratory). All strains were on the C57BL/6/129 background. Littermate MYC^{WT} mice were used as controls. For our MYC$^{\Delta M}$ mice bone phenotype study, 12-week-old

male ($n = 11$ per group) and female ($n = 6$ per group) MYC^ΔM and littermate control MYC^WT mice were used. For our OVX-induced bone loss study in MYC^ΔM mice, 13-week-old MYC^ΔM mice and their littermate MYC^WT mice were randomly divided into sham-operated or ovariectomized groups ($n ≥7$ per group) and were housed in the facility for 6 weeks after the operation. To examine in vitro oxidative phosphorylation in the ERRα-deficient condition, 8-week-old *Esrra*-deficient male mice and control mice were purchased from The Jackson Laboratory. To analyze the therapeutic effect of XCT790 (R&D Systems), 11-week-old sham-operated or ovariectomized C3H mice ($n ≥4$ per group) and CD-1 mice ($n ≥5$ per group) from Charles River Laboratories were randomized and treated with either vehicle or XCT790 (5 mg/kg for C3H mice and 2.5 mg/kg for CD-1 mice) i.p. once per day for 6 weeks, beginning 3 weeks after the operation. XCT790 was prepared in 10% KLEPTOSE (Roquette Pharma) following the manufacturer's instructions.

Analysis of bone phenotype. μCT analysis (44) was performed as described previously (45), and all samples were included in the analysis, which was conducted in a blinded manner. For μCT analysis, a Scanco Medical μCT 35 System with an isotropic voxel size of 7 μm was used to image the distal femur. Scans were conducted in 70% ethanol and used an x-ray tube potential of 55 kVp, an x-ray intensity of 0.145 mA, and an integration time of 600 ms. For analysis of femoral bone mass, a 2.1-mm-wide region of trabecular bone was contoured, starting 280 μm from the proximal end of the distal femoral growth plate. A total of 250 slices were read in each sample. Femoral trabecular bone was thresholded at 211 per mille. Femoral cortical bone was thresholded at 350 per mille. A Gaussian noise filter optimized for murine bone was applied to reduce noise in the thresholded 2D image. 3D reconstructions were created by stacking the thresholded 2D images from the contoured region. For histopathological assessment, femurs were fixed in 4% paraformaldehyde for 3 days. These samples were decalcified with 10% neutral buffered EDTA (Sigma-Aldrich) and embedded in paraffin. To assess osteoclastogenesis and bone resorption, sections were stained with tartrate-resistant acid phosphatase (TRAP) and hematoxylin for osteoclast visualization on trabecular bone within the femur metaphysis. All measurements were performed using Osteometric software (Osteomeasure) according to standard procedures (46) and were confined to the secondary spongiosa and restricted to an area between 400 and 2,000 mm distal to the growth plate metaphyseal junction of the distal femur. Osteoclasts were identified as TRAP-positive cells that were multinucleated and adjacent to bone.

Reagents. Human M-CSF and RANKL were purchased from Peprotech. The ERRα inverse agonist XCT790 was purchased from R&D Systems. The metabolic inhibitors 2-deoxy-D-glucose (2-DG), 6-diazo-5-oxo-L-norleucine (DON), and oligomycin, and the MYC inhibitor 10058-F4 were purchased from Sigma-Aldrich. The antibodies used for immunoblotting were as follows: NFATc1 (BD Pharmingen; 556602); MYC, ERRα, and β3 integrin (Cell Signaling Technology; 5605, 13826, and 4702); p38α (Santa Cruz Biotechnology Inc.; sc535); α-tubulin (Sigma-Aldrich; T9026); lamin B and PGC1β (Abcam; ab16048 and ab176328); phosphorylated ERK1/2 (p-ERK1/2), IκBα, and p-p38 (Cell Signaling Technology; 9101, 9242, and 9215); and tGFP (Origene; TA150041).

Osteoclast differentiation. Bone marrow cells were flushed from the femurs of mice, followed by lysis of rbc using ammonium chloride potassium (ACK) lysis buffer (Cambrex). The surviving cells were cultured in α-MEM supplemented with 10% FBS and 5% L929 cell supernatant, which served as as a source of M-CSF (47). The nonadherent cell population was recovered the next day and cultured with M-CSF–containing conditioned medium (CM) for 3 additional days. The final concentration of M-CSF in our culture was 23.3 ng/ml. We defined this cell population as mouse OCPs. For osteoclastogenesis assays, mouse OCPs were plated at a seeding density of $1 × 10^4$ per well in triplicate wells on a 96-well plate and incubated with M-CSF–containing CM and RANKL (50 ng/ml) for an additional 3 days, with exchange of fresh M-CSF–containing CM and RANKL every 2 days. Cells were fixed and stained for TRAP using the Acid Phosphatase Leukocyte Diagnostic Kit (Sigma-Aldrich) as recommended by the manufacturer. Multinucleated (>3 nuclei) TRAP-positive osteoclasts were counted in triplicate wells.

Bone resorption pit assays. The bone resorption activity of osteoclasts was examined using 96-well Corning Osteo Assay Surface Plates (Sigma-Aldrich). Mouse OCPs were plated at a seeding density of $1 × 10^4$ per well and incubated with M-CSF–containing CM and RANKL (50 ng/ml) for 10 days, with exchange of fresh M-CSF–containing CM and RANKL every 2 days. After removing cells with 10% bleach solution, plates were stained with 1% toluidine blue solution to visualize the formation of pits. The resorbed area was analyzed using OsteoMeasure software (OsteoMetrics).

Retroviral overexpression. The appropriate retroviral constructs as described in the Supplemental Methods were transfected into a packaging cell line, Plat-E, using FuGENE HD Transfection Reagent (Promega), and then the viral supernatant was collected after 48 hours of incubation. The filtered virus-containing supernatant was mixed with equal volumes of α-MEM containing 20% FBS in the presence of 6 μg/ml polybrene (Santa Cruz Biotechnology Inc.) along with 10% M-CSF–containing CM and then added to OCPs. After 24 hours of viral incubation, OCPs were used for experiments.

RNA preparation and real-time PCR. DNA-free RNA was obtained using the RNeasy Mini Kit (QIAGEN) with DNase treatment, and 0.5 μg total RNA was reverse transcribed using a First Strand cDNA Synthesis Kit (Thermo Fisher Scientific). Real-time PCR was performed in triplicate using the iCycler iQ Thermal Cycler and Detection System (Applied Biosystems) following the manufacturer's protocol. Expression of the tested gene was normalized relative to levels of hypoxanthine guanine phosphoribosyl transferase (*Hprt*) for mice and TATA box–binding protein (*TBP*) for humans. The primer sequences are listed in Supplemental Table 1.

RNA-seq. Total RNA was first extracted. TruSeq Sample Preparation Kits (Illumina) were then used to purify poly-A transcripts and generate libraries with multiplexed barcode adaptors. All samples passed quality control analysis on a Bioanalyzer 2100 (Agilent Technologies). Paired-end reads ($50 × 2$ cycles, $~75 × 10^6$ reads per sample) were obtained on an Illumina HiSeq 2500 at the Weill Cornell Medical College Genomics Resources Core Facility. The TopHat program (version 2.0.11) was used to align the reads to the mm10 mouse reference genome, while the Cufflinks program (version 2.2.0) allowed for measurements of transcript abundance (represented by fragments per kilobase of exon model per million mapped reads [FPKM]). Genes and transcripts with FPKM values below 5 were not included in the analysis. Pearson's correlation analysis was performed, and heatmaps were generated using R (version 3.0.2). Data from 2 biological replicates were used for bioinformatics analysis.

Mitochondrial oxygen consumption measurement. The real-time mitochondrial OCR and extracellular acidification rate (ECAR) were measured using the XF96 Extracellular Flux Analyzer (Seahorse Bioscience) with the Cell Mito Stress Kit (Seahorse Bioscience) following the manufacturer's instructions. The measurement was normalized to the relative level of DNA determined by measuring the fluorescence intensity of cells stained by SYTO 24 Green Fluorescent Nucleic Acid Stain (Molecular Probes). Briefly, OCPs were seeded on XF96 cell culture microplates (Seahorse Bioscience) at a seeding density of 8×10^3 cells per well and stimulated with RANKL (50 ng/ml) for 2 days. Before the assay, cells were rinsed twice and kept in prewarmed XF assay medium (pH 7.4) supplemented with 1 mM sodium pyruvate, 2 mM glutamine, and 10 mM glucose in a 37°C non-CO_2 incubator for 1 hour. Next, the respiratory rate was measured at 37 °C in at least 3 replicates per condition by using the following perturbation drugs in succession: 1 μM oligomycin, 2 μM carbonyl cyanide-*p* trifluoromethoxyphenyl-hydrazone (FCCP), and 0.5 μM rotenone/antimycin A. The basal OCR was measured before drug exposure. We calculated the mitochondrial function metrics as described in Supplemental Figure 9 and as directed in the Cell Mito Stress Kit manual (Seahorse Bioscience).

Accession numbers. The RNA-seq data were deposited in the NCBI's Sequence Read Archive (SRA) under accession number SRP096890.

Statistics. All statistical analyses were performed with GraphPad Prism 5.0 (GraphPad Software) using a 2-tailed, unpaired *t* test (2 conditions) or 1- or 2-way ANOVA for multiple comparisons (>2 conditions) with Tukey's post-hoc test. A *P* value of less than 0.05 was considered statistically significant.

Address correspondence to: Kyung-Hyun Park-Min; 535 East 70th Street, New York, New York 10021, USA. Phone: 212.774.7631; Email: ParkminK@hss.edu.

1. Nie Z, et al. c-Myc is a universal amplifier of expressed genes in lymphocytes and embryonic stem cells. *Cell*. 2012;151(1):68–79.
2. Lin CY, et al. Transcriptional amplification in tumor cells with elevated c-Myc. *Cell*. 2012;151(1):56–67.
3. Rahl PB, et al. c-Myc regulates transcriptional pause release. *Cell*. 2010;141(3):432–445.
4. Baudino TA, et al. c-Myc is essential for vasculogenesis and angiogenesis during development and tumor progression. *Genes Dev*. 2002;16(19):2530–2543.
5. Dang CV. MYC on the path to cancer. *Cell*. 2012;149(1):22–35.
6. Battaglino R, Kim D, Fu J, Vaage B, Fu XY, Stashenko P. c-myc is required for osteoclast differentiation. *J Bone Miner Res*. 2002;17(5):763–773.
7. Indo Y, et al. Metabolic regulation of osteoclast differentiation and function. *J Bone Miner Res*. 2013;28(11):2392–2399.
8. Park-Min KH, et al. Inhibition of osteoclastogenesis and inflammatory bone resorption by targeting BET proteins and epigenetic regulation. *Nat Commun*. 2014;5:5418.
9. Takayanagi H. Osteoimmunology: shared mechanisms and crosstalk between the immune and bone systems. *Nat Rev Immunol*. 2007;7(4):292–304.
10. Lorenzo J, Horowitz M, Choi Y. Osteoimmunology: interactions of the bone and immune system. *Endocr Rev*. 2008;29(4):403–440.
11. Takayanagi H. The role of NFAT in osteoclast formation. *Ann N Y Acad Sci*. 2007;1116:227–237.
12. Aliprantis AO, et al. NFATc1 in mice represses osteoprotegerin during osteoclastogenesis and dissociates systemic osteopenia from inflammation in cherubism. *J Clin Invest*. 2008;118(11):3775–3789.
13. Charles JF, et al. The collection of NFATc1-dependent transcripts in the osteoclast includes numerous genes non-essential to physiologic bone resorption. *Bone*. 2012;51(5):902–912.
14. Ikeda K, Takeshita S. The role of osteoclast differentiation and function in skeletal homeostasis. *J Biochem*. 2016;159(1):1–8.
15. Jin Z, Wei W, Yang M, Du Y, Wan Y. Mitochondrial complex I activity suppresses inflammation and enhances bone resorption by shifting macrophage-osteoclast polarization. *Cell Metab*. 2014;20(3):483–498.
16. Nishikawa K, et al. DNA methyltransferase 3a regulates osteoclast differentiation by coupling to an S-adenosylmethionine-producing metabolic pathway. *Nat Med*. 2015;21(3):281–287.
17. Zeng R, Faccio R, Novack DV. Alternative NF-κB Regulates RANKL-Induced Osteoclast Differentiation and Mitochondrial Biogenesis via Independent Mechanisms. *J Bone Miner Res*. 2015;30(12):2287–2299.
18. Ishii KA, et al. Coordination of PGC-1beta and iron uptake in mitochondrial biogenesis and osteoclast activation. *Nat Med*. 2009;15(3):259–266.
19. Wei W, et al. PGC1beta mediates PPARgamma activation of osteoclastogenesis and rosiglitazone-induced bone loss. *Cell Metab*. 2010;11(6):503–516.
20. Wan Y. PPARγ in bone homeostasis. *Trends Endocrinol Metab*. 2010;21(12):722–728.
21. Wei W, et al. Ligand Activation of ERRα by Cho-lesterol Mediates Statin and Bisphosphonate Effects. *Cell Metab*. 2016;23(3):479–491.
22. Clausen BE, Burkhardt C, Reith W, Renkawitz R, Förster I. Conditional gene targeting in macrophages and granulocytes using LysMcre mice. *Transgenic Res*. 1999;8(4):265–277.
23. Pello OM, et al. In vivo inhibition of c-MYC in myeloid cells impairs tumor-associated macrophage maturation and pro-tumoral activities. *PLoS One*. 2012;7(9):e45399.
24. Charles JF, Hsu LY, Niemi EC, Weiss A, Aliprantis AO, Nakamura MC. Inflammatory arthritis increases mouse osteoclast precursors with myeloid suppressor function. *J Clin Invest*. 2012;122(12):4592–4605.
25. Subramanian A, et al. Gene set enrichment analysis: a knowledge-based approach for interpreting genome-wide expression profiles. *Proc Natl Acad Sci USA*. 2005;102(43):15545–15550.
26. Carnesecchi J, Vanacker JM. Estrogen-Related Receptors and the control of bone cell fate. *Mol Cell Endocrinol*. 2016;432:37–43.
27. Bonnelye E, Aubin JE. An energetic orphan in an endocrine tissue: a revised perspective of the function of estrogen receptor-related receptor alpha in bone and cartilage. *J Bone Miner Res*. 2013;28(2):225–233.
28. Huss JM, Garbacz WG, Xie W. Constitutive activities of estrogen-related receptors: Transcriptional regulation of metabolism by the ERR pathways in health and disease. *Biochim Biophys Acta*. 2015;1852(9):1912–1927.
29. Busch BB, et al. Identification of a selective inverse agonist for the orphan nuclear receptor

estrogen-related receptor alpha. *J Med Chem*. 2004;47(23):5593–5596.

30. Villena JA, Kralli A. ERRalpha: a metabolic function for the oldest orphan. *Trends Endocrinol Metab*. 2008;19(8):269–276.

31. Yuk JM, et al. Orphan Nuclear Receptor ERRα Controls Macrophage Metabolic Signaling and A20 Expression to Negatively Regulate TLR-Induced Inflammation. *Immunity*. 2015;43(1):80–91.

32. Dang CV. Therapeutic targeting of Myc-reprogrammed cancer cell metabolism. *Cold Spring Harb Symp Quant Biol*. 2011;76:369–374.

33. Chen BJ, Wu YL, Tanaka Y, Zhang W. Small molecules targeting c-Myc oncogene: promising anti-cancer therapeutics. *Int J Biol Sci*. 2014;10(10):1084–1096.

34. Zaidi M. Skeletal remodeling in health and disease. *Nat Med*. 2007;13(7):791–801.

35. Raisz LG. Pathogenesis of osteoporosis: concepts, conflicts, and prospects. *J Clin Invest*. 2005;115(12):3318–3325.

36. Novack DV, Teitelbaum SL. The osteoclast: friend or foe? *Annu Rev Pathol*. 2008;3:457–484.

37. Rosen CJ. Clinical practice. Postmenopausal osteoporosis. *N Engl J Med*. 2005;353(6):595–603.

38. Wang R, et al. The transcription factor Myc controls metabolic reprogramming upon T lymphocyte activation. *Immunity*. 2011;35(6):871–882.

39. Novack DV, et al. The IkappaB function of NF-kappaB2 p100 controls stimulated osteoclastogenesis. *J Exp Med*. 2003;198(5):771–781.

40. Vaira S, et al. RelB is the NF-kappaB subunit downstream of NIK responsible for osteoclast differentiation. *Proc Natl Acad Sci U S A*. 2008;105(10):3897–3902.

41. Yang C, et al. NIK stabilization in osteoclasts results in osteoporosis and enhanced inflammatory osteolysis. *PLoS One*. 2010;5(11):e15383.

42. Teyssier C, et al. Absence of ERRalpha in female mice confers resistance to bone loss induced by age or estrogen-deficiency. *PLoS One*. 2009;4(11):e7942.

43. Gallet M, et al. Repression of osteoblast maturation by ERRα accounts for bone loss induced by estrogen deficiency. *PLoS One*. 2013;8(1):e54837.

44. Bouxsein ML, Boyd SK, Christiansen BA, Guldberg RE, Jepsen KJ, Müller R. Guidelines for assessment of bone microstructure in rodents using micro-computed tomography. *J Bone Miner Res*. 2010;25(7):1468–1486.

45. Shim JH, et al. Schnurri-3 regulates ERK downstream of WNT signaling in osteoblasts. *J Clin Invest*. 2013;123(9):4010–4022.

46. Parfitt AM, et al. Bone histomorphometry: standardization of nomenclature, symbols, and units. Report of the ASBMR Histomorphometry Nomenclature Committee. *J Bone Miner Res*. 1987;2(6):595–610.

47. Englen MD, Valdez YE, Lehnert NM, Lehnert BE. Granulocyte/macrophage colony-stimulating factor is expressed and secreted in cultures of murine L929 cells. *J Immunol Methods*. 1995;184(2):281–283.